nature nanotechnology

SUPPLEMENTARY INFORMATION
https://doi.org/10.1038/s41565-018-0162-7

In the format provided by the authors and unedited.

Switchable geometric frustration in an artificial-spin-ice–superconductor heterosystem

Yong-Lei Wang[1,2,3,7]*, Xiaoyu Ma[2,7], Jing Xu[1,4,7], Zhi-Li Xiao[1,4]*, Alexey Snezhko[1], Ralu Divan[5], Leonidas E. Ocola[5,6], John E. Pearson[1], Boldizsar Janko[2]* and Wai-Kwong Kwok[1]

[1]Materials Science Division, Argonne National Laboratory, Argonne, IL, USA. [2]Department of Physics, University of Notre Dame, Notre Dame, IN, USA. [3]Research Institute of Superconductor Electronics, School of Electronic Science and Engineering, Nanjing University, Nanjing, China. [4]Department of Physics, Northern Illinois University, DeKalb, IL, USA. [5]Center for Nanoscale Materials, Argonne National Laboratory, Argonne, IL, USA. [6]Present address: IBM Thomas J. Watson Research Center, Yorktown Heights, NY, USA. [7]These authors contributed equally: Yong-Lei Wang, Xiaoyu Ma, Jing Xu. *e-mail: yongleiwang@nju.edu.cn; xiao@anl.gov; bjanko@nd.edu

Supplementary Figures

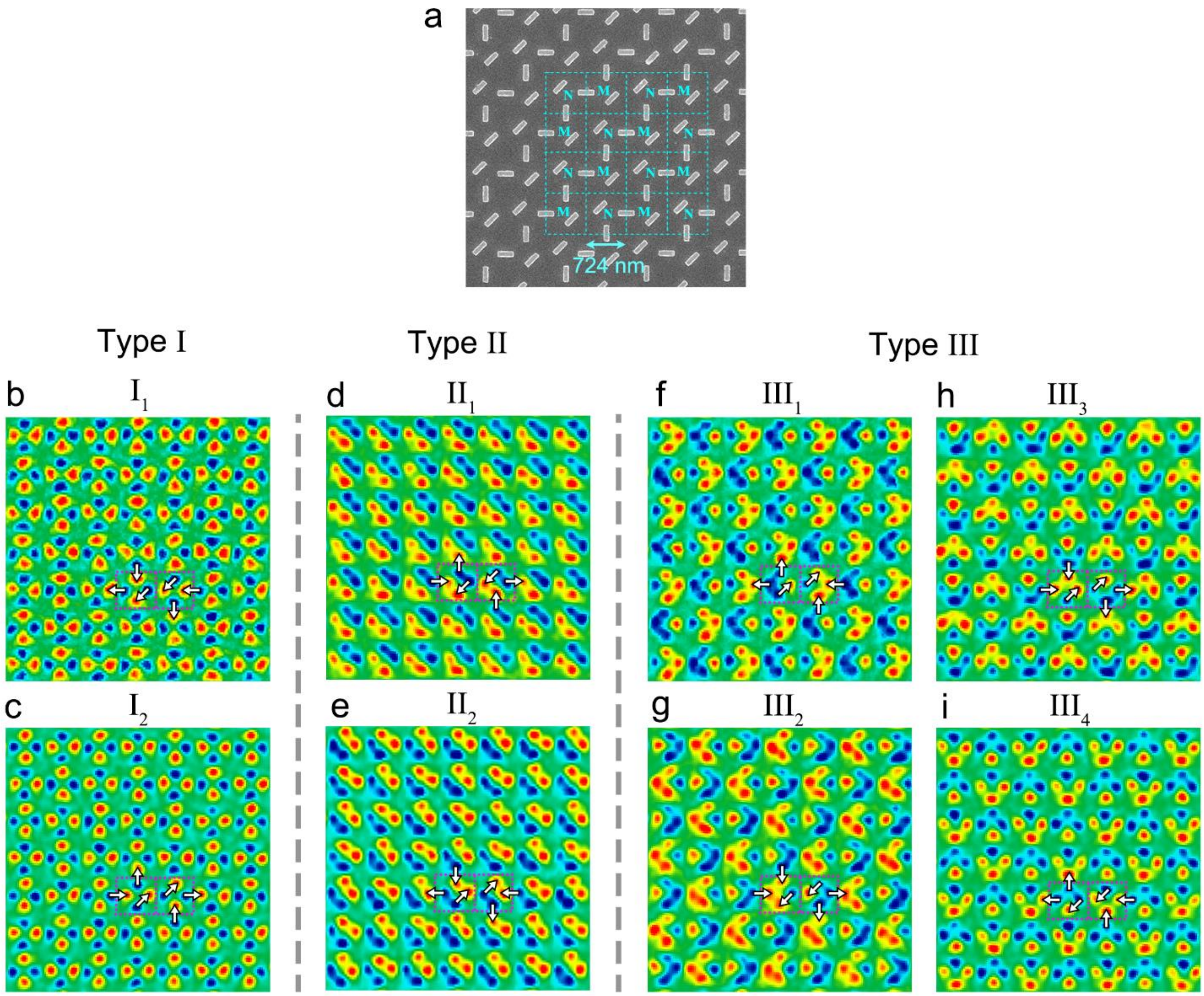

Supplementary Fig. 1 | All eight possible configurations of long range magnetic charge ordering. a, Scanning electron microscopy image of the tri-axial artificial-spin-ice patterned on top of a MoGe film. Two sublattices are labeled with M and N, respectively. The square lattice constant is about 724 nm. The dimension of the nano-bar magnets is 300 nm×80 nm×25 nm. **b-i**, Magnetic force microscopy images of eight configurations of ordered magnetic charges obtained from the tri-axial artificial-spin-ice structure (a) in our hetero-structure. The red and blue spots denote positive and negative magnetic charges, respectively. The purple boxes outline the M and N plaquettes defined in Fig. 1b. The arrows indicate the spin configuration of the nanoscale bar magnets.

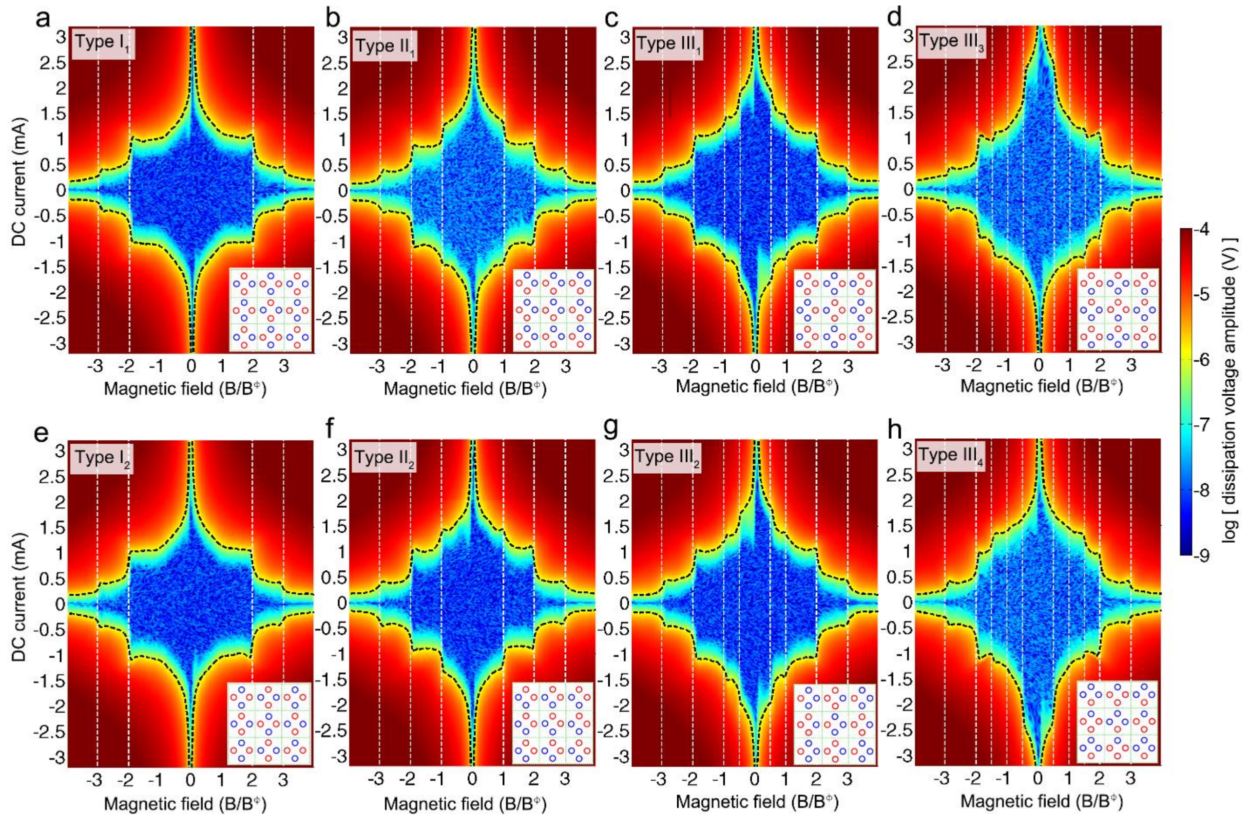

Supplementary Fig. 2 | Magnetic field matching effect for all eight possible configurations of magnetic charges. Color maps of the magnetic field and current dependent voltage. The corresponding magnetic charge configurations are presented in the insets. The current is in the horizontal direction. The magnetic field is perpendicular to the sample surface. The unit B^{Φ} = 40 Oe corresponds to one flux quantum per square plaquette. The black dashed lines indicate the magnetic field dependent critical current curves defined by a voltage criterion of 1 µV. The voltage maps are symmetric with magnetic field polarity for all the magnetic charge configurations. They are symmetric with current polarity for Type I_1 (a), I_2 (e), III_1 (c) and III_2 (g) charge configurations and asymmetric with current polarity for Type II_1 (b), II_2 (f), III_3 (d) and III_4 (h) charge configurations. The magnetic charge polarities of Type I_1, II_1, III_1 and III_3 (a-d) are reversed (positive charges to negative charges and vice versa) as compared to those of Type I_2, II_2, III_2 and III_4 (e-h), respectively. This leads to the results at positive current in (a-d) equal to those at negative current (e-h) respectively and vice versa (The flux-quanta move oppositely for positive and negative currents).

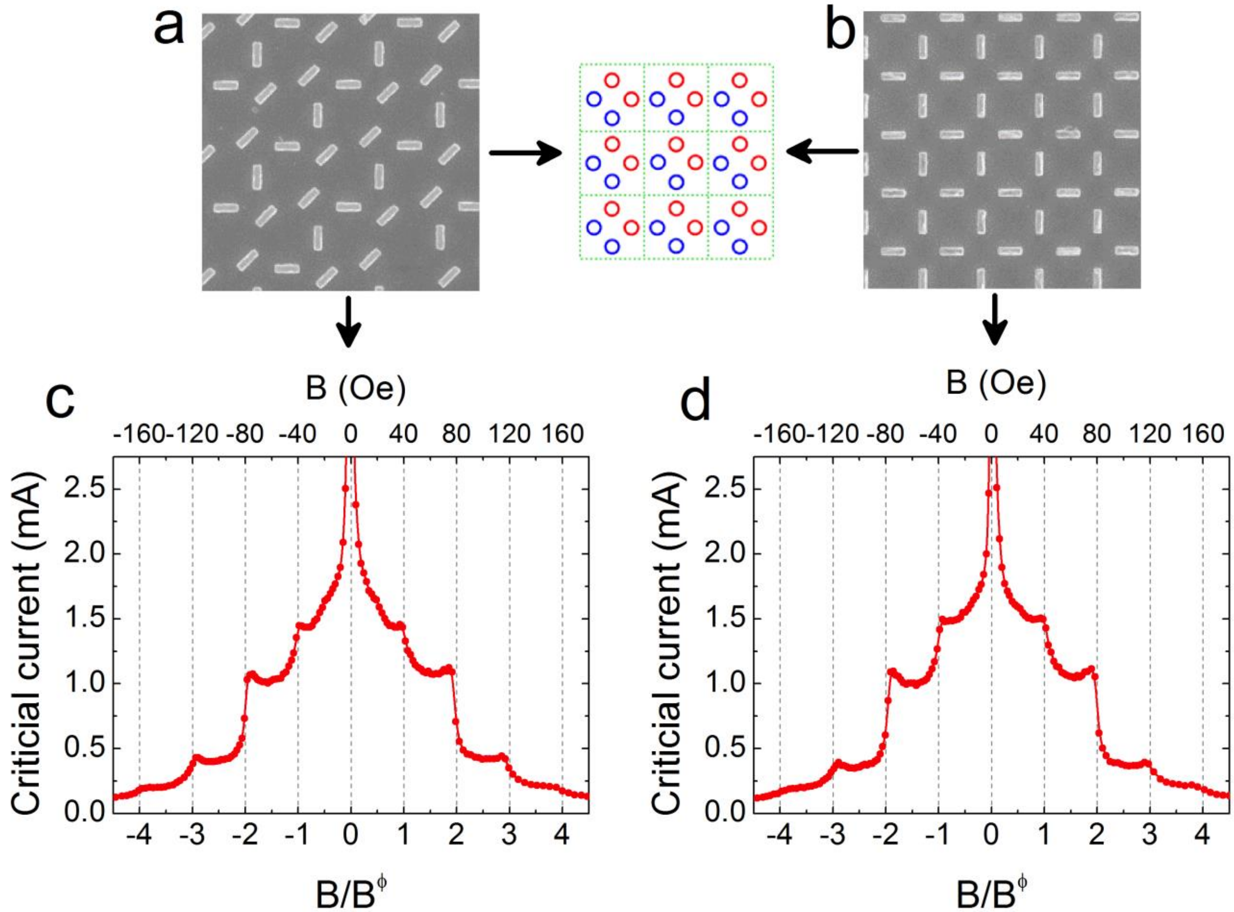

Supplementary Fig. 3 | Magnetic charge driven flux-quanta matching effect. a,b, Scanning electron microscopy images of our tri-axial artificial-spin-ice structure (**a**) which enables in-plane field control of the three sub-lattice oriented nanomagnets compared with a typical square artificial-spin-ice structure (**b**) in which Type-II magnetic charge order can be obtained by diagonally polarized in-plane magnetic field. **c,d**, Magnetic field dependent critical current curves measured from tri-axial artificial-spin ice (**c**) and square artificial-spin-ice (**d)** on a superconducting film under identical Type-II magnetic charge configurations shown in the middle. Both artificial-spin-ice structures show nearly identical matching effects.

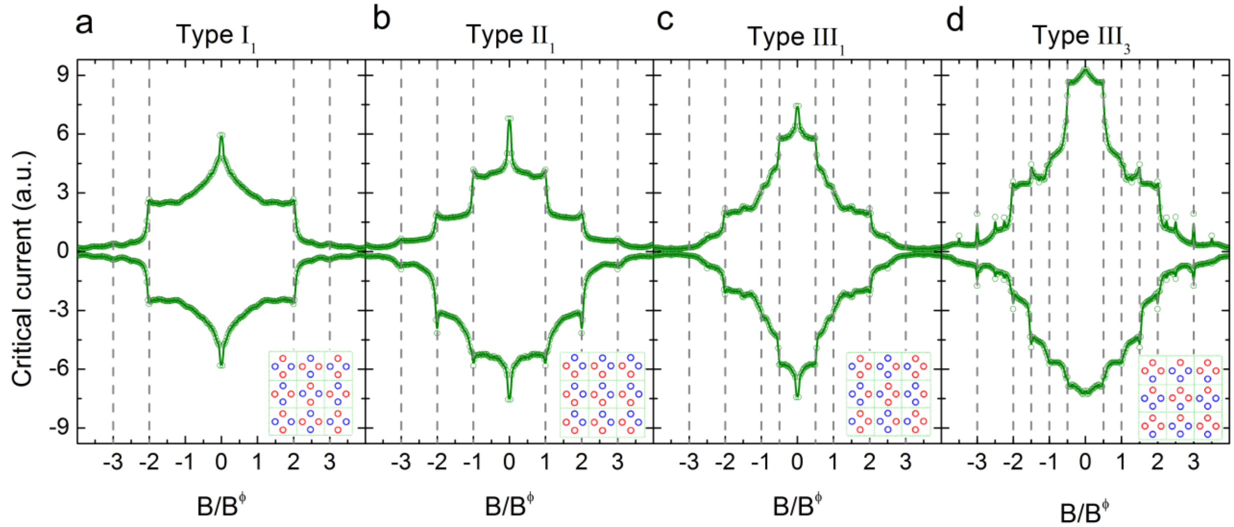

Supplementary Fig. 4 | Simulated magnetic field dependent critical currents for Type I, II and III magnetic charge order configurations. a-d, corresponds to experimental results in Supplementary Figure 2a-2d, respectively. The insets show the associated magnetic charge configurations.

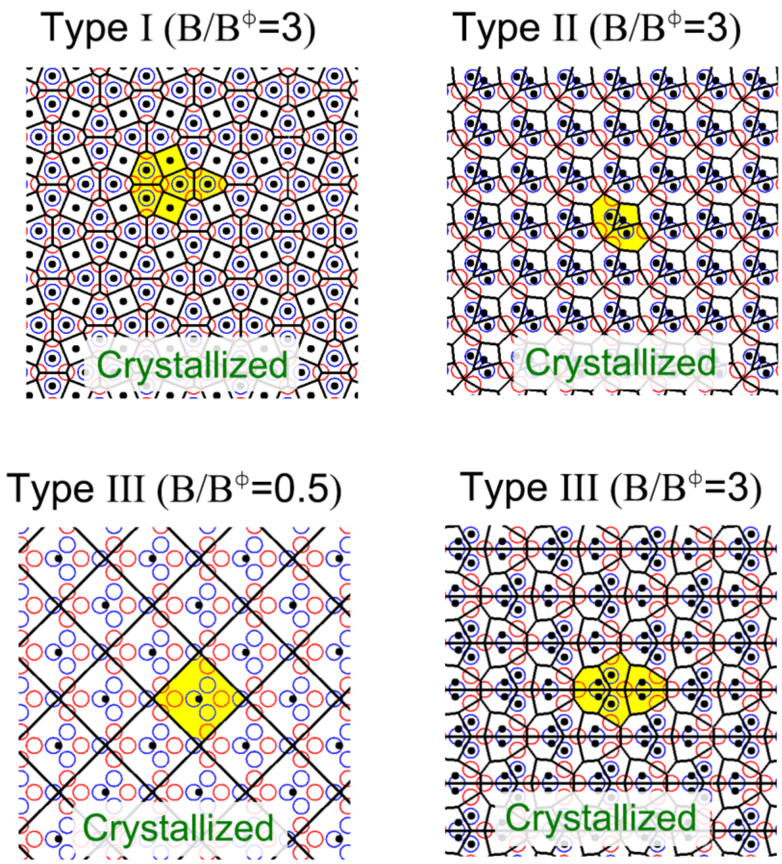

Supplementary Fig. 5 | Several more simulated distributions of flux-quanta. The magnetic charge configurations and magnetic field are listed above each image.

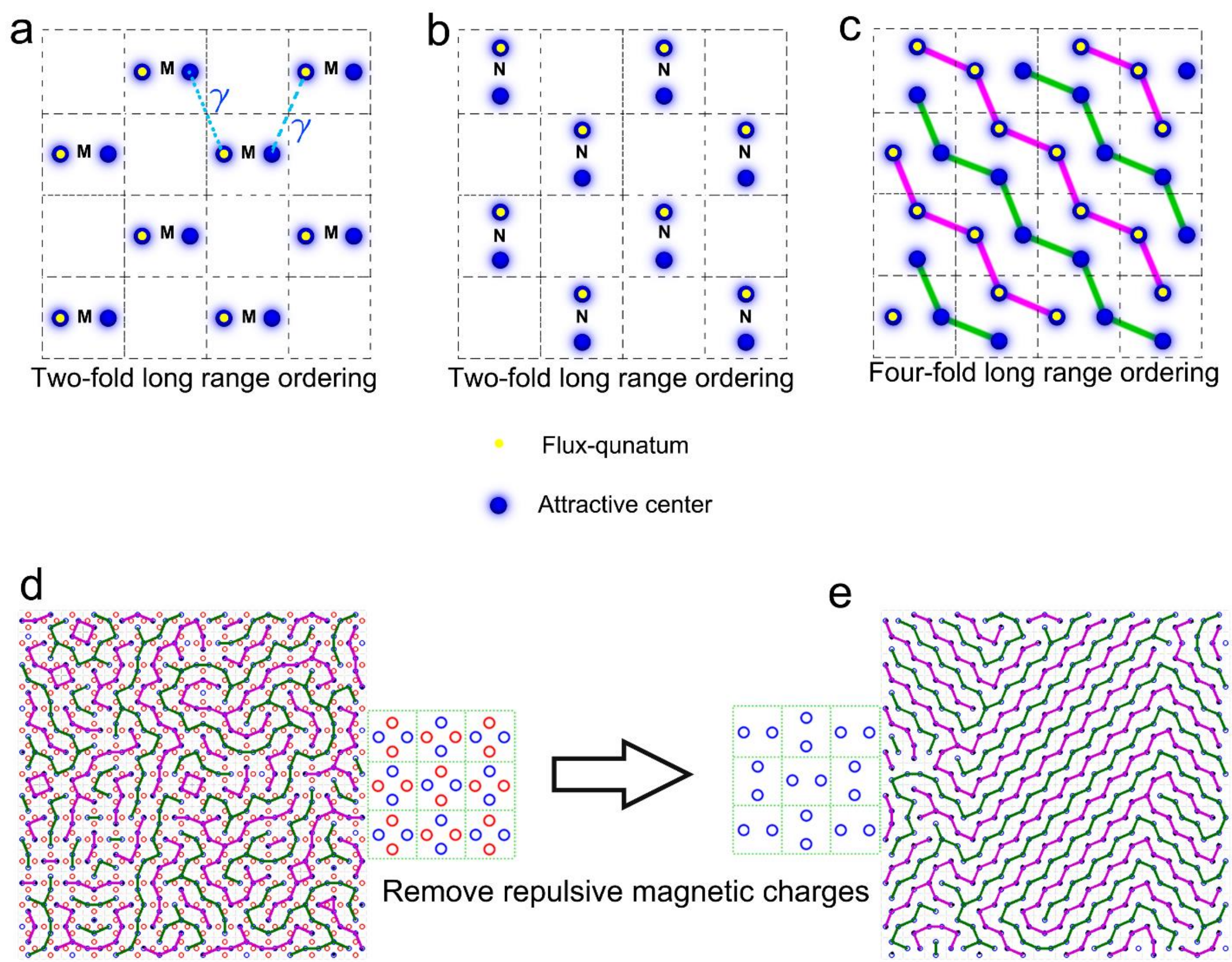

Supplementary Fig. 6 | Emergence of long range ordered flux-quanta when the repulsive potential centers are removed. a,b, sublattices containing only M plaquettes (a) or N plaquettes (b). The favorable 'one filled, one empty' configuration can be satisfied for all γ pairs when the flux-quanta all fill either the left or right attractive centers in each M plaquette (top or bottom attractive centers in each N plaquette), leading to a two-fold long range ordering of flux-quanta in each sublattice. **c**, four-fold long range ordering of flux-quanta in a full lattice (both M and N plaquettes) satisfies all γ pairs in the favorable 'one filled, one empty' configuration. The Labyrinth patterns obtained by connecting frustrated α and β pairs of 'two filled' (purple) and 'two empty' (green) show stripe-like long range ordering of flux-quanta. **d,e**, The disordered flux-quanta (random Labyrinth patterns) induced by Type-I charge order with both attractive and repulsive centers transform into long range ordered flux-quanta (large domains of stripe-like Labyrinth patterns) when the repulsive centers are removed.

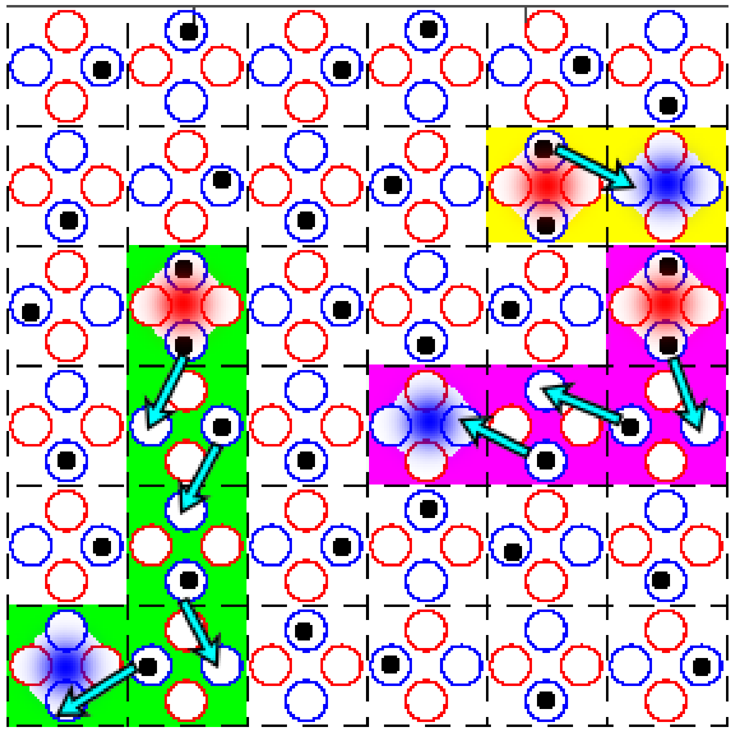

Supplementary Fig. 7 | Flux-quanta ‘monopoles’ and ‘Dirac strings’. The frustrated α pair in each square plaquette has a net flux-quantum ‘charge’ of +1 and -1 for ‘two filled’ and ‘two empty’ α pairs, respectively, as highlighted by the red and blue central spots. Three Dirac strings connecting a pair of positive and negative flux quanta ‘charges’ are shown in green, yellow and purple colors, respectively. The arrows show possible flux-quanta motion leading to annihilation of the positive and negative flux quanta ‘charges’.

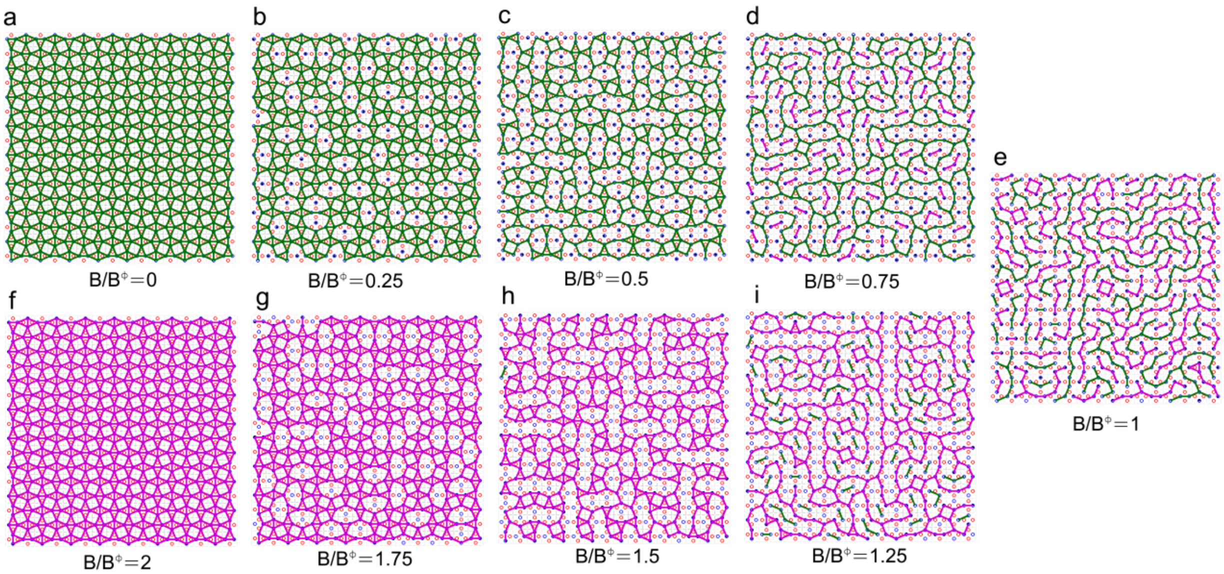

Supplementary Fig. 8 | Evolution of magnetic field dependent geometric frustration and crystallization under Type I charge order. Labyrinth patterns obtained by connecting frustrated α and β pairs (see Fig. 3c for pair definition) 'two filled' (purple) and 'two empty' (green) show distributions of the flux-quanta and the competing energies (green: FQ/MC interaction energy; purple: inter-FQs interaction energy) at various magnetic fields (or flux-quanta density) listed below each figure. The number of filled (empty) attractive centers in the top panels (a-d) equal to that of the empty (filled) attractive centers in the bottom panels (f-i), respectively. The $B/B^{\Phi} = 1$ pattern shows highly frustrated configuration while the $B/B^{\Phi} = 0$ and 2 show perfectly ordered patterns.

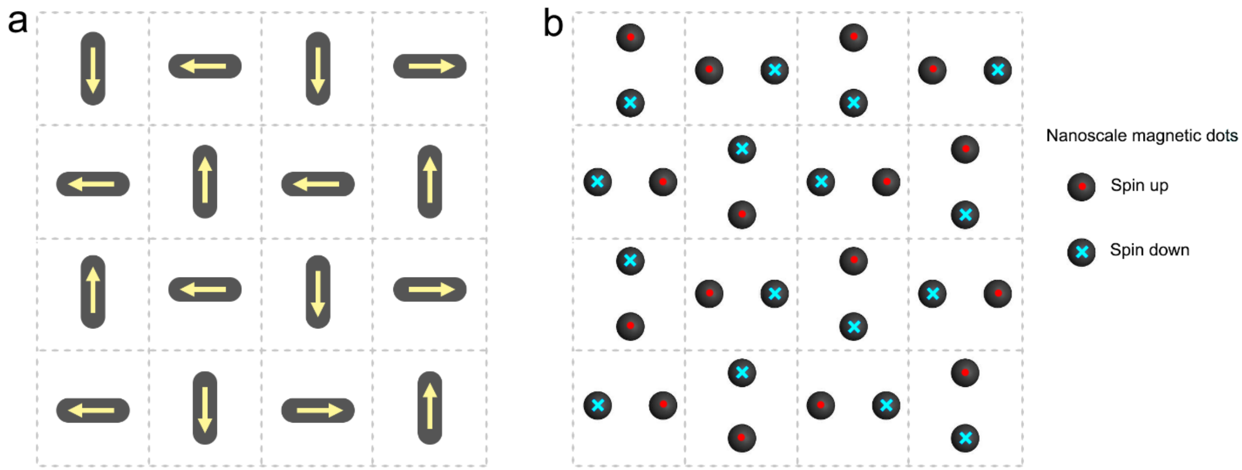

Supplementary Fig. 9 | Artificial-spin-ice analog of the new geometric frustration in our flux-quantum system. a, an array of nanoscale bar magnets. **b**, an array of nanoscale magnetic dots with out-of-plane anisotropy.

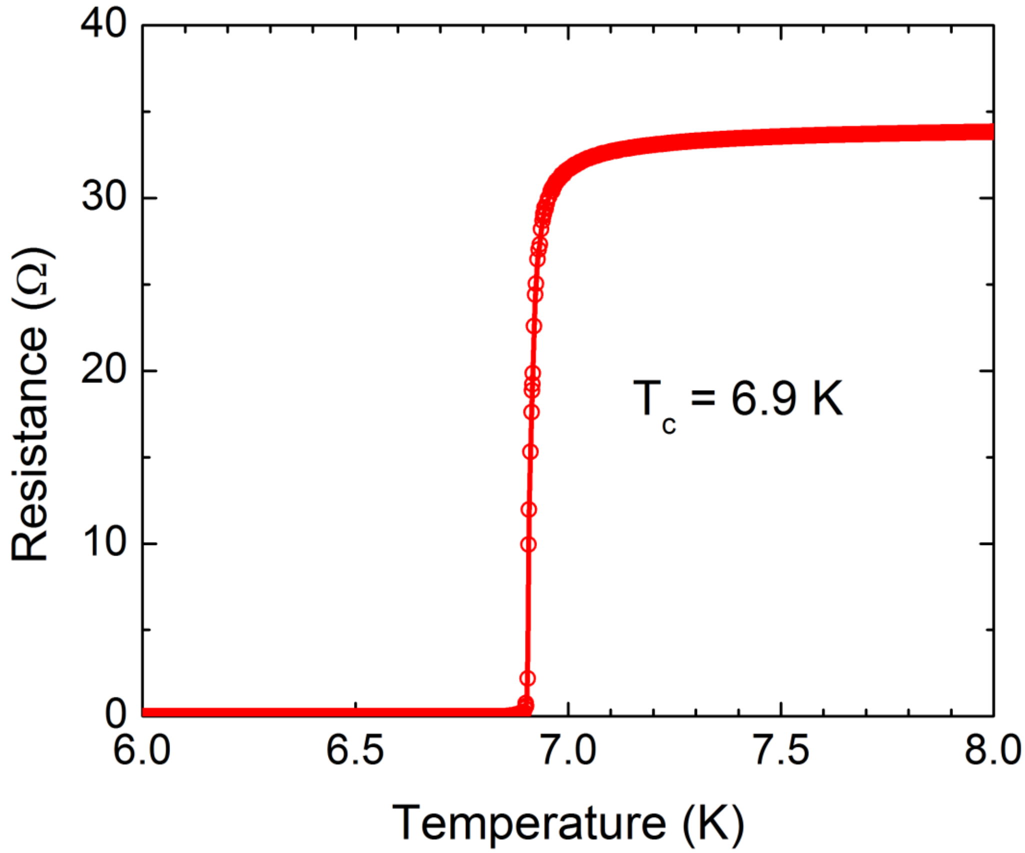

Supplementary Fig. 10 | Temperature dependent resistance. The resistance versus temperature curve displays a sharp superconducting transition with a critical temperature of $T_c \approx$ 6.9 K. The resistance was measured with an applied current of 100 μA under zero external magnetic field.

Supplementary Movie Captions

Supplementary Movie 1 | DC Transport Property under Type-II MC Configuration at $\boldsymbol{B/B^{\Phi}}$ = 1.5

Movie showing asymmetric DC transport behavior of FQs under Type-II MC configuration at $B/B^{\Phi} = 1.5$. With the same current amplitude, FQs move more easily in one direction than the other. This leads to ratchet motion of FQs as well as a DC dissipation voltage response under AC driving current. FQs are represented by black dots. Color map shows relative amplitude of pinning potential, with positive for repulsive potentials and negative for attractive potentials.

Supplementary Movie 2 | DC Transport Property under Type-III MC Configuration at $\boldsymbol{B/B^{\Phi}}$ = 0.5

Movie showing asymmetric DC transport behavior of FQs under Type-III MC configuration at $B/B^{\Phi} = 0.5$. The representations are the same as those in Movie 1.

Supplementary Movie 3 | DC Transport Property under Type-III MC Configuration at $\boldsymbol{B/B^{\Phi}}$ = 1.0

Movie showing asymmetric DC transport behavior of FQs under Type-III MC configuration at $B/B^{\Phi} = 1.0$. Combined with Movie 2, it shows reversible DC transport behavior of FQs at different flux quanta density.